The Astrophysical Journal, 591:1086–1096, 2003 July 10

CONSTRAINING THE STRUCTURE OF GAMMA-RAY BURST JETS THROUGH THE AFTERGLOW LIGHT CURVES

Jonathan Granot
Institute for Advanced Study, Princeton, NJ 08540; granot@ias.edu

and

Pawan Kumar
Department of Astronomy, University of Texas, Austin, TX 78731; pk@surya.as.utexas.edu
Received 2002 November 13; accepted 2003 March 6

ABSTRACT

We investigate the effect that the structure of gamma-ray burst (GRB) jets has on the afterglow light curves for observers located at different viewing angles, $\theta_{\rm obs}$, from the jet symmetry axis. The largest uncertainty in the jet dynamics is the degree of lateral energy transfer. Thus, we use two simple models that make opposite and extreme assumptions for this point and calculate the light curves for an external density that is either homogeneous or decreases as the square of the distance from the source. The Lorentz factor, Γ, and kinetic energy per unit solid angle, ϵ, are initially taken to be power laws of the angle θ from the jet axis: $\epsilon \propto \theta^{-a}$, $\Gamma \propto \theta^{-b}$. We perform a qualitative comparison between the resulting light curves and afterglow observations. This constrains the jet structure, and we find that $a \approx 2$ and $0 \lesssim b \lesssim 1$ are required to reproduce typical afterglow light curves. Detailed fits to afterglow data are needed to determine whether a "universal" jet model, in which all GRB jets are assumed to be intrinsically identical and differ only by our viewing angle, $\theta_{\rm obs}$, is consistent with current observations.

Subject headings: gamma rays: bursts — gamma rays: theory — radiation mechanisms: nonthermal — relativity — shock waves

On-line material: color figures

1. INTRODUCTION

There are several different lines of evidence in favor of collimated outflows, also referred to as jets, in gamma-ray bursts (GRBs). Perhaps the best evidence so far is the achromatic break seen in the light curves of many (though not all) GRB afterglows. A collimated outflow also helps reduce the estimate for the total energy output in gamma rays that is inferred from the fluence in GRBs with known redshifts, which in some cases approaches and in one case (GRB 990123) even exceeds the rest energy of a solar-mass star, for a spherically symmetric emission. Such an energy output in gamma rays is hard to produce in any model that involves a stellar-mass object. Furthermore, a nonspherical flow can also manifest itself through linear polarization (Sari 1999; Ghisellini & Lazzati 1999), as was indeed observed for a few afterglows (Covino et al. 1999; Wijers et al. 1999; Rol et al. 2000).

Most GRB jet models consider an outflow that is uniform within some finite well-defined opening angle around its symmetry axis and where the Lorentz factor, energy density, etc., drop sharply beyond this opening angle (Rhoads 1997, 1999; Panaitescu & Mészáros 1999; Sari, Piran, & Halpern 1999; Kumar & Panaitescu 2000; Moderski, Sikora, & Bulik 2000; Granot et al. 2001, 2002). Such a uniform jet with a sharp well-defined edge shall be referred to as a top-hat jet. The possibility that GRB jets can display an angular structure, for which the kinetic energy per unit solid angle, ϵ, and the Lorentz factor, Γ, of the GRB outflow vary smoothly as power laws in the angle, θ, from the jet axis, was proposed by Mészáros, Rees, & Wijers (1998). We shall refer to such smoothly varying relativistic outflows as "structured" jets (as opposed to a top-hat jet, which has no inner structure).

Recently, several different groups have analyzed afterglow observations within the framework of the top-hat jet model and have inferred a relatively narrow distribution for both the total energy output in gamma rays (Frail et al. 2001) and the initial kinetic energy of the relativistic outflow (Panaitescu & Kumar 2001; Piran et al. 2001). These results may alternatively be interpreted as GRB jets having a universal structure, which is intrinsically the same for all GRBs, while the observed differences between different GRBs are a result of different viewing angle, $\theta_{\rm obs}$, with respect to the jet symmetry axis (Lipunov, Postnov, & Prokhorov 2001; Rossi, Lazzati, & Rees 2002; Zhang & Mészáros 2002). Whereas in the top-hat jet interpretation, the jet break time, t_j, depends mainly on the initial opening angle of the jet, θ_j (and also has a smaller dependence on its energy per unit solid angle and on the external density; e.g., Sari et al. 1999), in the universal "structured" jet interpretation t_j depends mainly on the viewing angle, $\theta_{\rm obs}$, and the light curve is similar to that for a top-hat jet with an opening angle $\theta_j = \theta_{\rm obs}$ and the same value of the energy per unit solid angle of the "structured" jet at $\theta = \theta_{\rm obs}$.

While the evolution of top-hat jets and their light curves have been widely investigated (Rhoads 1999; Panaitescu & Mészáros 1999; Kumar & Panaitescu 2000; Moderski et al. 2000; Granot et al. 2002), including numerical simulations of the jet dynamics and calculation of the resulting light curves (Granot et al. 2001), much less work has been done on "structured" jets. In an accompanying paper (Kumar & Granot 2003), we calculate the dynamics of "structured" relativistic jets by solving relativistic fluid dynamics equations and demonstrate that a simple analytic or semianalytic model can qualitatively reproduce the results for the jet dynamics and for the light curves as long as the Lorentz

factor along the jet axis is of order a few or larger. In this paper we use two simple models for the jet dynamics, which are designed to bracket the true hydrodynamic evolution of the jet, to calculate the afterglow light curves for a wide range of parameters for the structured jet and the external density. A qualitative comparison of the light curves with afterglow observations provides constraints on the jet structure and density profile in its immediate vicinity.

In § 2 we present the physical model. We begin with the initial conditions (§ 2.1), then describe our two simple dynamical models (§ 2.2), and finally outline the procedure for calculating the light curves (§ 2.3). Our results are presented in § 3, and in § 4 we discuss our main conclusions.

2. PHYSICAL MODEL

The jet is assumed to possess axial symmetry, so that all the hydrodynamic quantities at a given lab frame time, t, depend only on the angle, θ, from the jet symmetry axis. The radial profile of the outflow is ignored in this simple treatment, and the shocked material is approximated by a thin shell located at the same radius, R, as the shock.

The observed afterglow light curves depend on the angular structure of the GRB jet, its hydrodynamic evolution, and the viewing angle, $\theta_{\rm obs}$, with respect to the jet symmetry axis. One may therefore use the shape of the afterglow light curves to constrain the angular structure of the jet, as well as to infer the viewing angle, $\theta_{\rm obs}$. For a top-hat jet of opening angle θ_0, $\theta_{\rm obs} < \theta_0$ is required to observe the prompt gamma-ray emission. In this case the differences in the light curves between different $\theta_{\rm obs}$ in the range $0 \le \theta_{\rm obs} < \theta_0$ are rather small (Granot et al. 2001, 2002). However, for structured jets we expect large differences in light curves for different $\theta_{\rm obs}$.

2.1. *Initial Conditions*

The initial conditions are chosen at a lab frame time, t_0, for which, on the one hand, the internal shocks have ended, and on the other hand, no significant deceleration due to the sweeping up of the external medium has yet occurred [i.e., $R_{\rm IS}(\theta) < R(\theta, t_0) < R_{\rm dec}(\theta)$ for all relevant θ]. For simplicity, the original ejecta is assumed to remain cold, even near the deceleration radius, where it is expected to be heated by the passage of the reverse shock. This approximation might introduce inaccuracies of order unity near the deceleration epoch, corresponding to an observed time less than about a few minutes for a typical GRB, but it should have no effect on light curves at later times. Energy conservation implies

$$\epsilon(\theta, t_0) = \mu_0(\theta, t_0)[\Gamma(\theta, t_0) - 1] + \mu_s(\theta, t_0)\left[\Gamma^2(\theta, t_0) - 1\right] \approx \mu_0(\theta, t_0)\Gamma(\theta, t_0) , \quad (1)$$

where μ_0 and μ_s are the rest mass per unit solid angle of the original ejecta and of the swept-up external medium, respectively, ϵ is the energy (not including the energy associated with the rest mass) per unit solid angle in the outflow, Γ is the bulk Lorentz factor of the shocked material, and t_0 is chosen so that $\mu_s(\theta, t_0)\Gamma(\theta, t_0) \ll \mu_0(\theta, t_0)$ for all θ.

The initial kinetic energy per unit solid angle and initial Lorentz factor (minus 1) are assumed to be power laws in θ, outside a core of opening angle θ_c:

$$\epsilon(\theta, t_0) = \epsilon_0\Theta^{-a}, \quad \Gamma(\theta, t_0) = 1 + (\Gamma_0 - 1)\Theta^{-b} , \quad (2)$$

where ϵ_0 and Γ_0 are the initial kinetic energy per unit solid angle and Lorentz factor at the jet axis, and

$$\Theta \equiv \sqrt{1 + \left(\frac{\theta}{\theta_c}\right)^2} \approx \begin{cases} 1, & \text{for } \theta \ll \theta_c, \\ \theta/\theta_c, & \text{for } \theta \gg \theta_c. \end{cases} \quad (3)$$

The velocity is assumed to be in the radial direction, so that the initial radius is given by

$$R(\theta, t_0) = t_0\sqrt{1 - \Gamma^{-2}(\theta, t_0)} , \quad (4)$$

and the lateral transfer of matter can be neglected.[1] The external mass density profile is assumed to be a power law in the distance r from the source, $\rho_{\rm ext}(r) = Ar^{-k}$. This implies

$$\mu_s(\theta, t) = \int_0^{R(\theta,t)} r^2\, dr\, \rho_{\rm ext}(r) = \frac{AR(\theta, t)^{3-k}}{3-k} , \quad (5)$$

$$\mu_0(\theta, t) = \mu_0(\theta, t_0) = \frac{\epsilon_0\Theta^{b-a}}{\Gamma_0 - 1} - [\Gamma(\theta, t_0) + 1]\mu_s(\theta, t_0) . \quad (6)$$

2.2. *Jet Dynamics*

The main uncertainty in the jet dynamics is the degree of lateral transport of energy, from small to large angles, θ, with respect to the jet axis. We therefore make two alternative and extreme assumptions regarding this transport: in model 1 we assume that the energy per unit solid angle, ϵ, does not change with time, $\epsilon(\theta, t) = \epsilon(\theta, t_0)$, while in model 2 we assume the maximal averaging of ϵ over the angle θ that is consistent with causality. This is done by averaging over the initial distribution of ϵ,

$$\bar{\epsilon}(\theta, t) \equiv \frac{1}{\cos\theta_- - \cos\theta_+}\int_{\theta_-}^{\theta_+} d\theta'\, \sin\theta'\epsilon(\theta', t_0) , \quad (7)$$

where θ_- (θ_+) is the angle below (above) θ (i.e., $\theta_- < \theta < \theta_+$), to which a hypothetical sound wave that originated at θ at the initial time t_0 would have propagated. Initially, $\theta_-(t_0) = \theta_+(t_0) = \theta$, and these angles subsequently evolve according to

$$\frac{\partial\theta_\pm}{\partial t} = \pm\frac{c_s(\theta_\pm, t)}{\Gamma(\theta_\pm, t)R(\theta_\pm, t)}, \quad c_s = \sqrt{\frac{\hat{\gamma}(\hat{\gamma} - 1)[\Gamma - 1]}{1 + \hat{\gamma}[\Gamma - 1]}} , \quad (8)$$

where c_s is the local sound speed and $\hat{\gamma} = (4\Gamma + 1)/3\Gamma$ is the adiabatic index. This simple local scheme does not, in general, conserve the total energy in the outflow. The global energy conservation is imposed by renormalizing $\bar{\epsilon}$:

$$\epsilon(\theta, t) = \bar{\epsilon}(\theta, t)\frac{\int_0^{\pi/2} d\theta'\, \sin\theta'\epsilon(\theta', t_0)}{\int_0^{\pi/2} d\theta'\, \sin\theta'\bar{\epsilon}(\theta', t)} . \quad (9)$$

For both models 1 and 2, the radius of the thin shell of matter changes as[2]

$$\frac{\partial R(\theta, t)}{\partial t} = \sqrt{1 - \Gamma^{-2}(\theta, t)} , \quad (10)$$

[1] A more rigorous treatment of the jet hydrodynamics (Kumar & Granot 2003) shows that these assumptions are reasonable.

[2] There is a small difference between the velocity of the shock front and that of the fluid just behind the shock (Blandford & McKee 1976); however, for simplicity we neglect this distinction in the present treatment.

while μ_s and μ_0 are given by equations (5) and (6), respectively, and the Lorentz factor of the shocked material, Γ, is obtained by solving the equation for energy conservation,

$$\epsilon = (\Gamma - 1)\mu_0 + (\Gamma^2 - 1)\mu_s \, ,$$
$$\Gamma = \frac{\mu_0}{2\mu_s}\left[\sqrt{1 + \frac{4\mu_s(\epsilon + \mu_0 + \mu_s)}{\mu_0^2}} - 1\right] . \qquad (11)$$

2.3. *Light Curves*

The local emissivity is calculated using the conventional assumptions of synchrotron emission from relativistic electrons that are accelerated behind the shock into a power-law distribution of energies, $N(\gamma) \propto \gamma^{-p}$ for $\gamma > \gamma_m$, where the electrons and the magnetic field hold fractions ϵ_e and ϵ_B, respectively, of the internal energy. The shape of the local spectral emissivity is approximated as a broken power law with breaks at the typical synchrotron frequency ν_m and at the cooling frequency ν_c (Sari, Piran, & Narayan 1998). As our main focus in this work is the effect of the jet dynamics on the afterglow emission, we keep the expression for the local emissivity fairly simple and leave the inclusion of additional features such as the self-absorption frequency, inverse Compton emission and its effect on the electron cooling, etc., for later applications, since such complications might make it hard to pinpoint the effects of the jet dynamics on the light curves.

The light curves for observers located at different angles, $\theta_{\rm obs}$, with respect to the jet axis are calculated by applying the appropriate relativistic transformation of the radiation field from the local rest frame of the emitting fluid to the observer frames and integrating over equal photon arrival time surfaces (Granot, Piran, & Sari 1999; Kumar & Panaitescu 2000; Granot et al. 2001). The radiation calculation is in this sense rigorous and takes into account all relevant effects, so that the resulting light curves accurately reflect what is expected for a given jet structure and dynamics, where the latter are much less certain.

3. RESULTS

In Figures 1–3 we show the evolution of the hydrodynamic quantities according to the two models described in the previous section, for a constant-density external medium ($k = 0$). In Figure 1 we show the evolution of the Lorentz factor for $(a, b) = (0, 2)$. For $a = 0$, models 1 and 2 become identical, so that this figure applies to both models. Since $\epsilon(\theta, t) = \epsilon_0 = \text{const}$, the evolution after the deceleration time is the same for all θ, and different θ differ just by the deceleration time, $t_{\rm dec}$, and the corresponding deceleration radius, $R_{\rm dec}$, given by $\mu_s \sim \mu_0/\Gamma \sim \epsilon/\Gamma^2$, or

$$R_{\rm dec} = \left[\frac{(3-k)\epsilon_0}{Ac^2\Gamma_0^2}\right]^{1/(3-k)} \Theta^{(2b-a)/(3-k)} \, ,$$
$$t_{\rm dec} = \frac{R_{\rm dec}}{2c\Gamma^2(t_0)} \propto \Theta^{[2b(4-k)-a]/(3-k)} \, . \qquad (12)$$

As can be seen from equation (12), for $a = 0$, the deceleration occurs first at small θ, and gradually proceeds to larger angles. This can be nicely seen in Figure 1.

This situation is similar for $(a, b) = (2, 2)$, but is reversed for $(a, b) = (2, 0)$, as can be seen in Figures 2 and 3, where in the latter case the deceleration occurs first at large angles

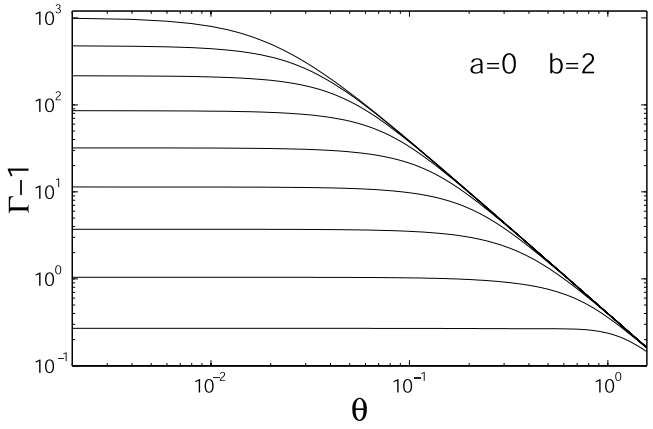

FIG. 1.—Evolution of the Lorentz factor $\Gamma(\theta) - 1$, for $(a, b) = (0, 2)$, $\Gamma_0 = 10^3$, and $\theta_c = 0.02$ rad. For $a = 0$, models 1 and 2 become the same, so that this figure applies to both models. [*See the electronic edition of the Journal for a color version of this figure.*]

θ and then proceeds to smaller angles. This is in agreement with equation (12). Figures 2 (*top*) and 3 (*top*) show the energy per unit solid angle, ϵ, which is initially the same for the two models, and remains unchanged for model 1, while for model 2 ϵ decreases at small angles θ, and increases at large angles. This indicates a lateral transfer of energy from small to large angles. At late times, as the flow becomes

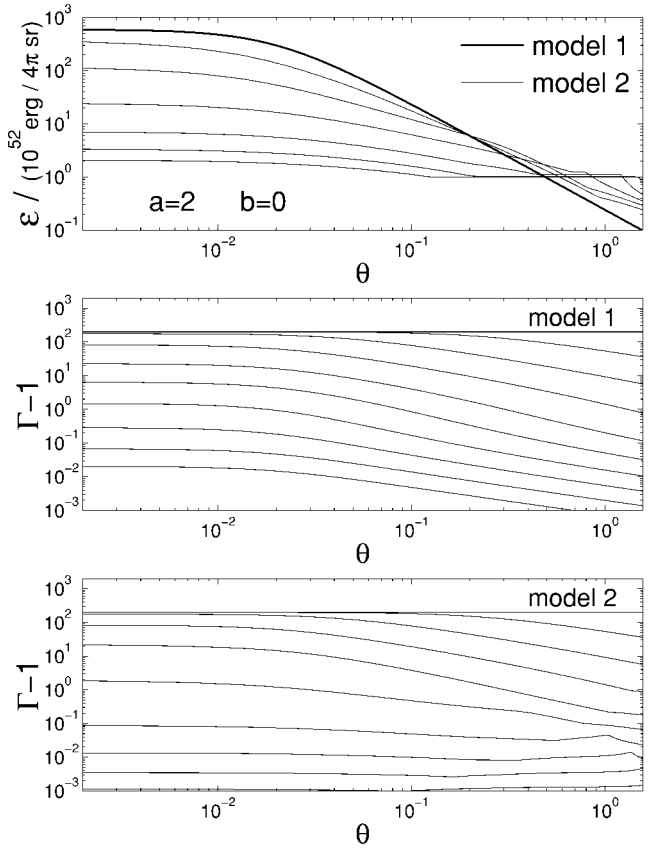

FIG. 2.—Hydrodynamic evolution of the energy per unit solid angle ϵ and the Lorentz factor $\Gamma - 1$ as a function of the angle θ from the jet symmetry axis, according to our two simple and extreme models, for $(a, b) = (2, 0)$. [*See the electronic edition of the Journal for a color version of this figure.*]

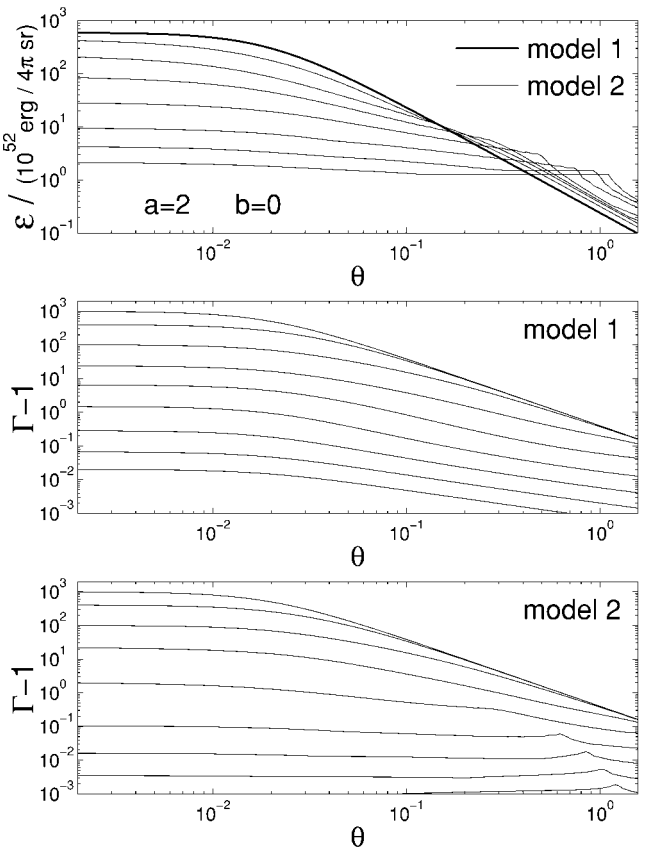

FIG. 3.—Same as Fig. 2 but for $(a, b) = (2, 2)$. [*See the electronic edition of the Journal for a color version of this figure.*]

subrelativistic, ϵ becomes almost independent of angle θ, and the flow approaches spherical symmetry, as is indeed expected to occur physically, since the spherically symmetric Sedov-Taylor self-similar solution should be asymptotically approached in the nonrelativistic regime. Figures 2 (*middle and bottom*) and 3 (*middle and bottom*) show the Lorentz factor minus 1, $\Gamma - 1$, for models 1 and 2, respectively. For model 1, it can be seen that while the flow is still relativistic, the Lorentz factor soon settles into a profile of $\Gamma - 1 \propto \theta^{-1}$ at $\theta > \theta_c$, instead of the initial $\Gamma - 1 \propto \theta^{-2}$ or $\Gamma = \text{const}$. This occurs since the fraction of the energy in the original ejecta soon becomes negligible, implying $\epsilon \approx \mu_s(\Gamma^2 - 1)$ so that as long as the flow is relativistic, $\mu_s \propto R^{3-k} \approx \text{const}$, since $R \approx ct$ for all θ and $\Gamma - 1 \propto \epsilon^{1/2} \propto \theta^{-1}$. When the flow becomes nonrelativistic, $\Gamma^2 - 1 \approx 2(\Gamma - 1) \approx \beta^2$ so that $\Gamma - 1 \propto \theta^{-4/(5-k)}$, which is still quite close to θ^{-1} for k between 0 and 2. For model 2, a similar effect is seen at early times, when $\epsilon(\theta, t) \approx \epsilon(\theta, t_0)$, but it becomes much more homogeneous at later times, as $\epsilon(\theta)$ becomes more uniform.

The light curves of models 1 and 2 for $(a, b) = (0, 0)$, $(0, 2)$, $(2, 0)$, and $(2, 2)$ and a uniform external medium $(k = 0)$ are shown in Figure 4, while the temporal decay slope, α (defined by $\alpha \equiv d \log F_\nu / d \log t$ or $F_\nu \propto t^\alpha$), for the same light curves is shown in Figure 5. We have added the spherical case, $(a, b) = (0, 0)$, for comparison. For $(a, b) = (0, 2)$, the light curve initially rises before the deceleration time, $t_{\rm dec}$, which occurs at latter times for larger viewing angles $\theta_{\rm obs}$, in accord with equation (12), when, keep in mind, the emission is dominated by $\theta \sim \theta_{\rm obs}$ at early times because of the relativistic beaming of the radiation emitted from the jet. After a time t, deceleration has occurred at $\theta < \theta_{\rm dec}(t)$, where $\theta_{\rm dec}$ is given by $t_{\rm dec}[\theta_{\rm dec}(t)] = t$, and the light curves for $\theta_{\rm obs} < \theta_{\rm dec}(t)$ approach the spherical case and hence become very close to one other. By keeping $a = 0$, ϵ, and Γ_0 fixed and increasing b from zero, $t_{\rm dec}(\theta_{\rm obs})$ begins to shift to larger times, and the ratio of the deceleration times for two given values of $\theta_{\rm obs}$ grows as b increases. Nevertheless, after the time $t_{\rm dec}(\theta_{\rm obs})$, the light curves still approach the same spherical light curve, for all values of b. There is no jet break in the light curve for $a = 0$. Since jet breaks are observed in many afterglows, this type of jet structure can be ruled out as a universal model for GRB jets.

For $(a, b) = (2, 0)$ and $(2, 2)$ we find a jet break in the light curve at roughly the same time as predicted in previous works (Rossi et al. 2002; Zhang & Mészáros 2002), i.e., when $\Gamma(\theta = \theta_{\rm obs}) \sim \theta_{\rm obs}^{-1}$. However, we also find some new and interesting features. For $(a, b) = (2, 2)$ with $\Gamma_0 \lesssim 10^3$, the initial Lorentz factor at large angles, θ, is quite modest, resulting in a large deceleration time, $t_{\rm dec}$, which can be as large as $t_{\rm dec} \gtrsim 1$ day for $\theta_{\rm obs} \gtrsim 0.2$. This would result in a rising light curve at early times, for all frequencies. On the other hand, for $(a, b) = (2, 0)$, where the initial Lorentz factor is the same for all θ, the deceleration time, $t_{\rm dec}$, is very small everywhere, so that the initial rise of the light curve at $t < t_{\rm dec}$ will be very hard to observe. The lack of an observation of a rising light curve for afterglow observations starting from a few hours after the burst can already constrain the jet structure: either $b < 2$ or $\Gamma_0 > 10^3$ are required. Future observations at much earlier times after the burst, as may be achieved with the forthcoming *Swift* mission, may provide much stronger constraints on the jet structure. Furthermore, the initial Lorentz factor along our line of sight should to be $\gtrsim 100$ in order to observe the prompt gamma-ray emission. Since it is very hard to accelerate the ejecta to a Lorentz factor above 10^4, or arguably, even above a few 10^3, this leaves at most two decades in $\Gamma(\theta, t_0)$ for angles θ from which the prompt GRB can be observed. Since the inferred range of viewing angles $\theta_{\rm obs}$ is at least one decade, this would imply $b < 2$ for a universal jet model.

It can also be seen from Figure 4 that for $(a, b) = (2, 2)$, the value of the temporal decay slope, α (defined by $F_\nu \propto t^\alpha$), before the jet break, is higher for larger viewing angles $\theta_{\rm obs}$. This effect is very large for model 1, but not very significant for model 2 (see Fig. 5). The value of α before the break in the light curve for model 1 is larger than the observed value for several well-studied GRB afterglows, and the light-curve power-law steepening, $|\delta\alpha|$, is smaller than the observed value for many GRBs. The light curves obtained using model 1 at early times are almost identical to the light curves from hydrodynamic simulations, and this suggests that jet structure described by $(a, b) = (2, 2)$ is not consistent with the observations for a number of GRBs. Therefore, a universal jet structure with $a = 2$ would require $0 \lesssim b \lesssim 1$.

For $(a, b) = (2, 0)$ the correlation between α before the jet break and $\theta_{\rm obs}$ is not seen, but instead there is a flattening of the light curve (i.e., an increase in α) just before the jet break, for viewing angles sufficiently large compared with the core angle of the jet, $\theta_{\rm obs} \gtrsim 3\theta_c$. This effect is more prominent in model 1, where it can also be seen to a lesser extent for $(a, b) = (2, 2)$ as well, compared with model 2, where this effect is smaller and can be seen only for $(a, b) = (2, 0)$ (see Fig. 5). Light curves calculated for the same jet profiles

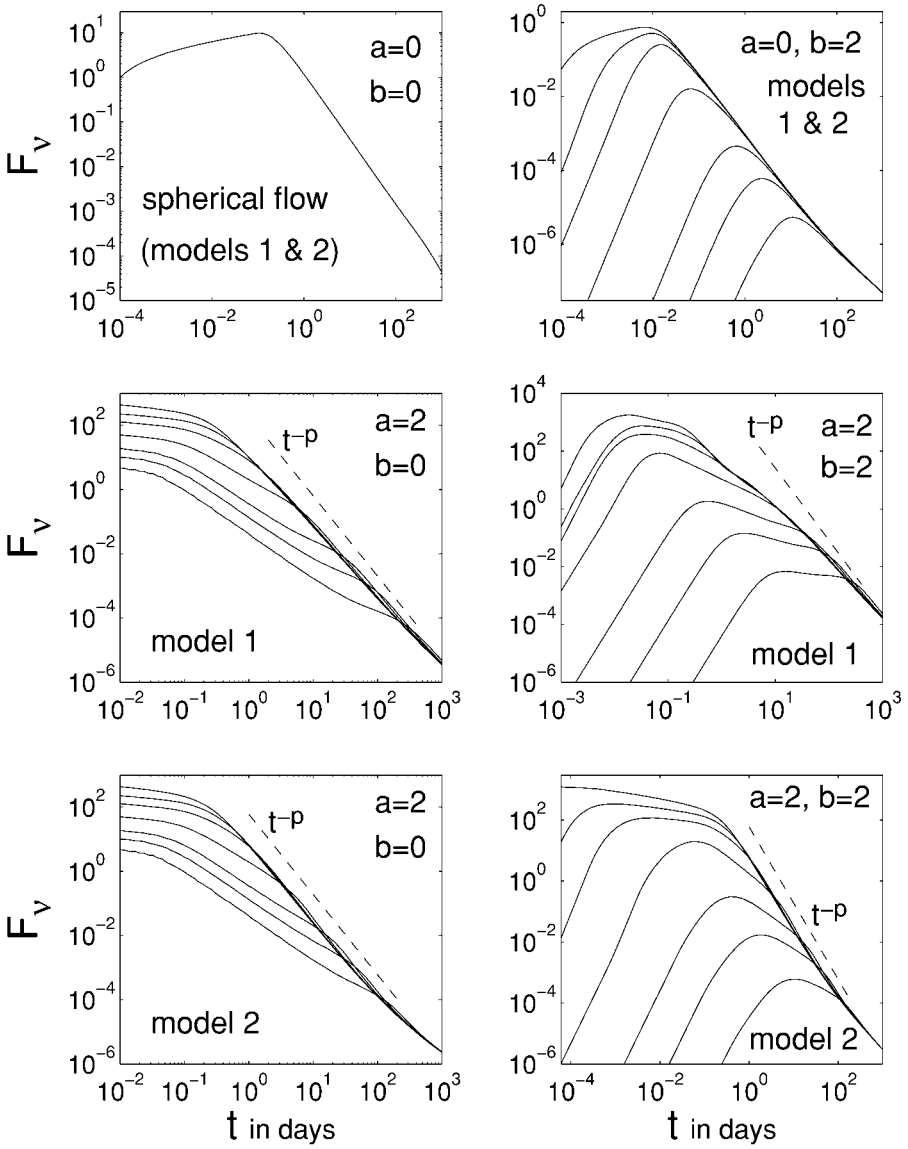

FIG. 4.—Light curves for a constant-density external medium ($k = 0$) for models 1 and 2 (see text for details) in the optical ($\nu = 5 \times 10^{14}$ Hz), for a jet core angle $\theta_c = 0.02$, viewing angles $\theta_{\rm obs} = 0.01, 0.03, 0.05, 0.1, 0.2, 0.3$, and 0.5, $p = 2.5$, $\epsilon_e = \epsilon_B = 0.1$, $n = 1$ cm^{-3}, $\Gamma_0 = 10^3$, and ϵ_0 chosen so that the total energy of the jet would be 10^{52} ergs. A power law of t^{-p} is added in some of the panels for comparison. [*See the electronic edition of the Journal for a color version of this figure.*]

but with the jet dynamics given by a hydrodynamic simulation (Kumar & Granot 2003) show that for $(a, b) = (2, 0)$ a reasonably sharp jet break is obtained only for $\theta_{\rm obs} \gtrsim (2-3)\theta_c$, while the flattening in the light curve just before the jet break becomes prominent at $\theta_{\rm obs} \gtrsim (5-7)\theta_c$. This leaves only a factor of $\sim$3 in $\theta_{\rm obs}/\theta_c$, for which there is a sharp jet break with no flattening in the light curve just before this break, as is seen in all afterglows with jet breaks. However, the inferred values of $\theta_{\rm obs}$ range at least 1 order of magnitude, $\theta_{\rm obs} \sim 2^\circ$–$20^\circ$. Therefore, $(a, b) = (2, 0)$ might have some difficulties as a universal jet profile, for all GRBs, since θ_c is expected to vary between different afterglows. Even without requiring a universal jet profile, i.e., the same θ_c for all GRB jets, it would be highly improbable if all viewing angles would by chance fall within the narrow range that gives a light curve qualitatively similar to observations. However, one should keep in mind that the flattening in the light curve is most pronounced at large viewing angles $\theta_{\rm obs}$, for which the flux around the jet break time is low and therefore hard to monitor, and the jet break occurs at late times when model 2, which shows a less pronounced flattening before the jet break, provides a better description of the jet dynamics. Therefore, a detailed comparison with afterglow data is required to determine whether all current observations can be explained in the context of a universal jet model.

In Figure 6 we show the light curves for $b = 0$ and $a = 1$, 2, and 3. It can be seen that the light curves for $a = 2$ have the largest resemblance to afterglow observations. For $a = 1$ the steepening of the light curve across the jet break is too small, and the light curve after the jet break is not steep enough. For $a = 3$ there is either a very pronounced flattening in the light curve before the jet break time, or the temporal decay slope after the jet break is extremely steep. Therefore, $a \approx 2$ is preferred from the shape of the light curves. This is consistent with the fact that $a = 2$ is required

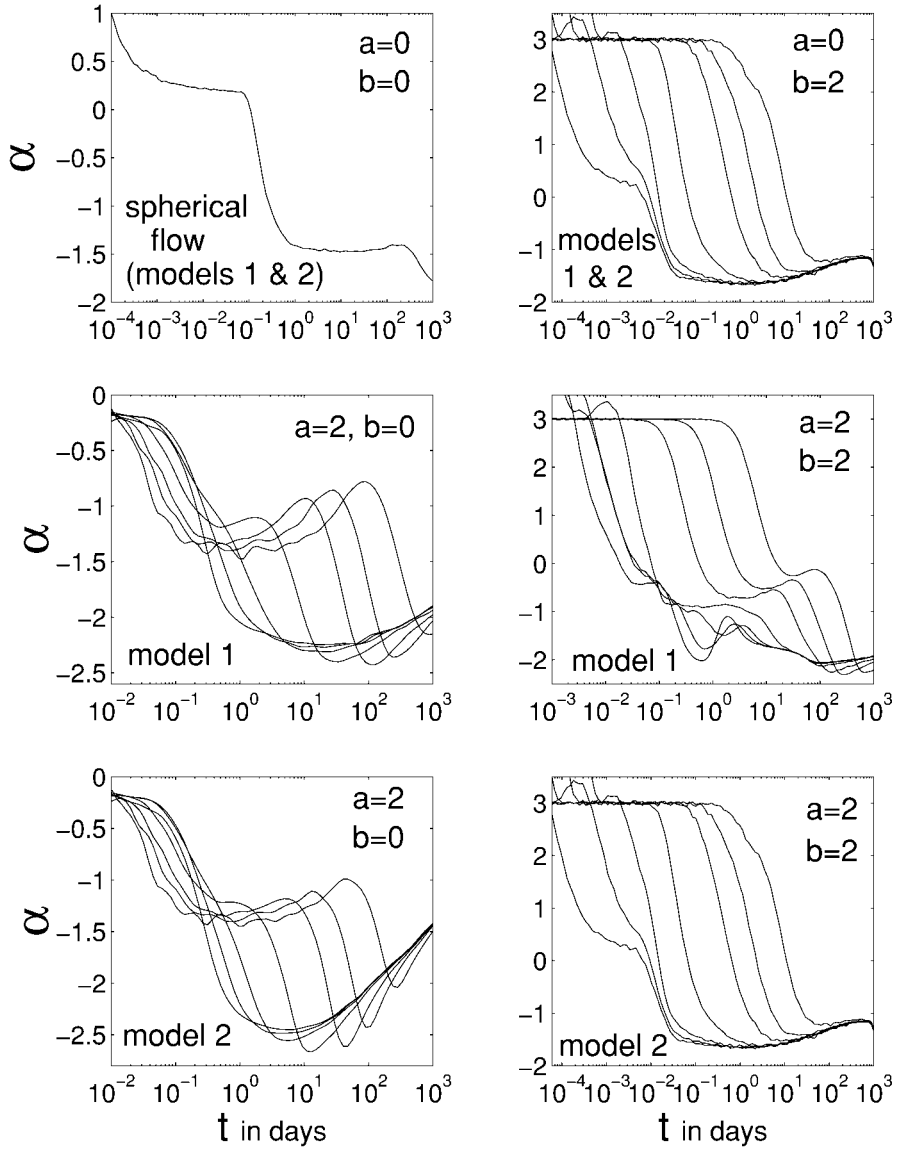

FIG. 5.—Temporal decay slope, $\alpha \equiv d \ln F_\nu / d \log t$ (i.e., $F_\nu \propto t^\alpha$), for the light curves shown in Fig. 4, for a constant-density environment ($k = 0$). [*See the electronic edition of the Journal for a color version of this figure.*]

to satisfy the correlation found by Frail et al. (2001) between the isotropic equivalent gamma-ray fluence in the GRB and the jet break time. However, the latter consideration is based on a statistical argument and has to assume a universal jet structure, while the former can be applied on a burst-to-burst basis and may be used to constrain the structure of an individual GRB with a well-monitored afterglow emission.

To see more clearly the differences between the light curves of models 1 and 2, we show them on top of each other in Figure 7, for $(a, b) = (2, 0)$. At times much smaller than the jet break time, $t \ll t_j$, the light curves for models 1 and 2 are practically the same, since very little lateral transfer of energy has occurred at $\theta \sim \theta_{\rm obs}$, from which the dominant contribution to the light curve is coming. At $t \gtrsim t_j$ the light curves of model 2 have a lower flux compared with those of model 1, since the lateral transfer of energy to larger angles θ becomes significant and reduces the energy per unit solid angle at small values of θ, which are responsible for most of the contribution to the light curve at the reasonably small viewing angles $\theta_{\rm obs}$ that we consider (and that are also of most interest). At very late times, when the flow becomes nonrelativistic, the emission from the whole jet can be seen from all viewing angles, and relativistic beaming becomes unimportant, causing the light curves at all $\theta_{\rm obs}$ to become similar and decreasing the differences between the light curves of models 1 and 2. At this late stage the flow is expected to become spherically symmetric, as indeed happens in model 2, but not in model 1. Therefore model 2 is more realistic at late times. Model 2 shows less flattening of the light curve before the jet break and has a slightly earlier jet break time compared with model 1.

Figure 8 shows the light curves for an external density that drops as r^{-2} ($k = 2$). This corresponds to a stellar wind of a massive star progenitor. In the pulsar wind bubble model of GRBs, the effective external density can have a different profile, which may be approximated as a power law with an index k that ranges between 0 and 1 (Königl & Granot 2002). Therefore $k = 0$ and $k = 2$ are the extreme values of k that may be expected, and an intermediate value

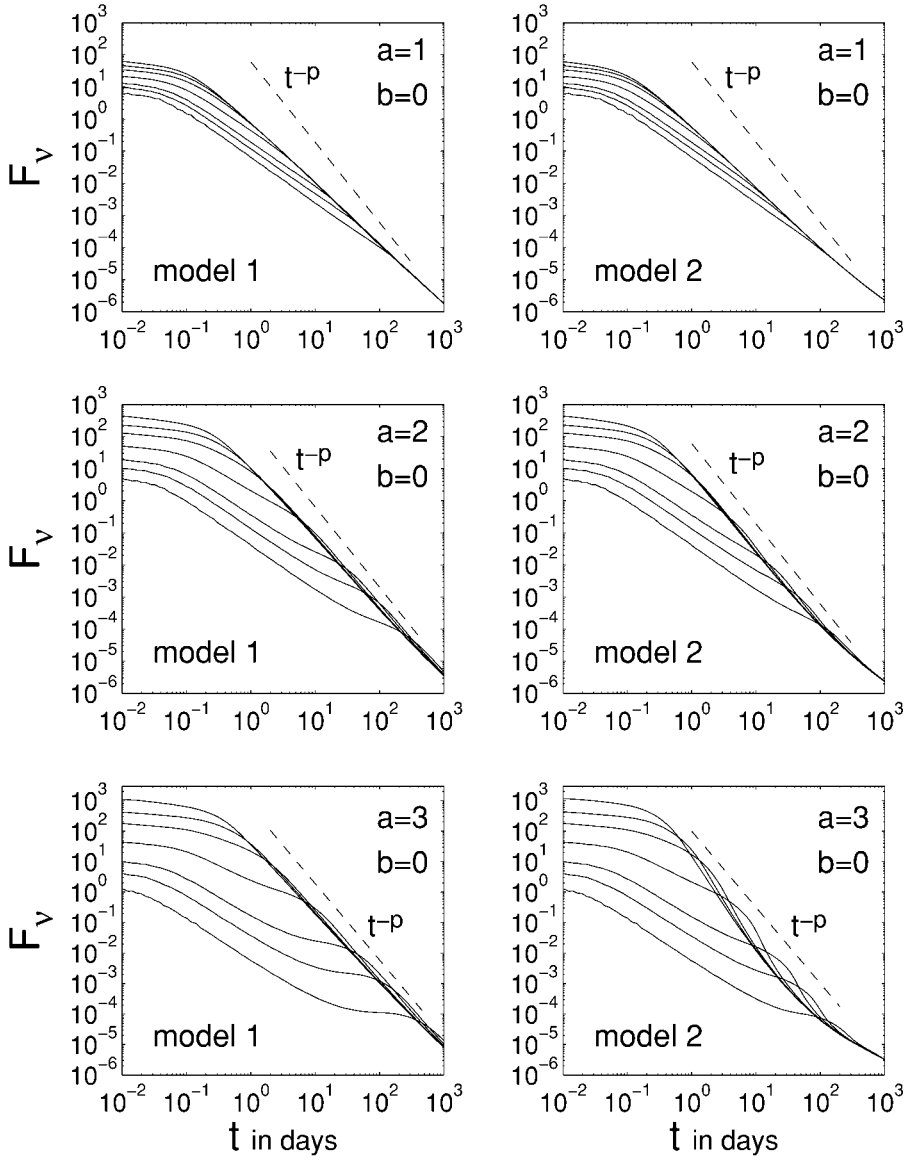

FIG. 6.—Same as Fig. 4, but for a constant initial Lorentz factor, $\Gamma(t_0) = 200$, independent of θ ($b = 0$), and for three different values for the power-law index, a, of the initial distribution of the energy per unit solid angle, ϵ ($a = 1$, 2, and 3). [*See the electronic edition of the Journal for a color version of this figure.*]

of k, resulting in an intermediate behavior of the light curves, is possible.

For $k = 2$ we see a break in the light curve for a spherical flow ($a = b = 0$) at $t \sim 10$ yr, corresponding to the nonrelativistic transition time, $t_{\rm NR}$. This can also be seen in Figure 9, which shows the temporal decay slope, α, for the same light curves shown in Figure 8. Generally, $t_{\rm NR} \propto E^{1/(3-k)}$, so that for $k = 2$ it is linear in E, and a more moderate total energy of, say, 10^{51} ergs would give $t_{\rm NR} \sim 1$ yr. We extend the observer time for which we show the light curves to illustrate that in the nonrelativistic regime all light curves become similar. One should keep in mind that physically one may expect an r^{-2} external density profile only up to some finite radius (for a stellar wind, this corresponds to the radius of the wind termination shock) while at much larger radii we expect a roughly constant-density medium. This would result in modifications to the light curves shown here; however, this is typically expected to affect the light curves only in the nonrelativistic regime ($t \gtrsim t_{\rm NR}$).

The deceleration time, $t_{\rm dec}$, is typically very small for $k = 2$ since the density at small radii is very large, and the total swept-up mass is only linear in radius. The jet break is much smoother and less sharp compared with a constant-density environment ($k = 0$), as was found for a top-hat jet considered by Kumar & Panaitescu (2000). There is a relatively sharp break only for $(a, b) = (2, 0)$, and even then it is hardly sharp enough to reproduce the jet breaks observed in GRB afterglows. This suggests $k < 2$, or rather $k \lesssim 1$. It is interesting to note that this is consistent with the external density profile expected in the pulsar wind bubble model (Königl & Granot 2002; Guetta & Granot 2003), while this is not consistent with the density profile expected in the collapsar model, $k = 2$.

4. DISCUSSION

We have calculated light curves from structured relativistic jets (jets whose Lorentz factor and energy per unit solid

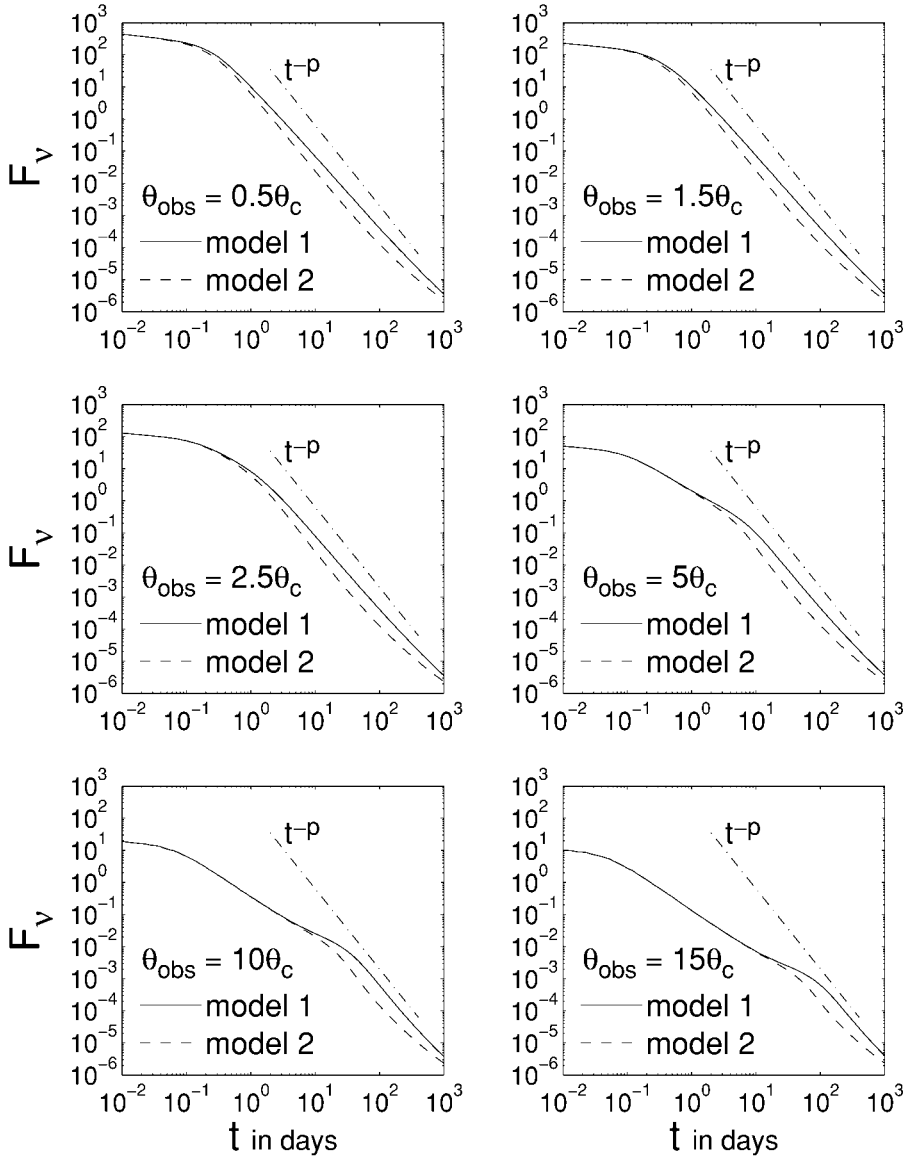

FIG. 7.—Light curves for $(a, b) = (2, 0)$, for which the remaining parameters are the same as in Fig. 4. Each panel corresponds to a different viewing angle, and the light curves for models 1 and 2 are shown together to make it easier to compare the two models. [*See the electronic edition of the Journal for a color version of this figure.*]

angle vary smoothly with angle from the jet axis), using two simple models for the jet dynamics, motivated by the hydrodynamic simulation of Kumar & Granot (2003), and as two limiting cases of energy redistribution in the lateral direction.

The first model considers the energy per unit solid angle, $\epsilon(\theta, t)$, to be time independent, so that each segment of the jet evolves independently of the other parts of the jet, as if it was part of a spherical flow. This is roughly consistent with the results from hydrodynamic simulations of structured jets for which ϵ varies slowly with θ, in which we find the transverse velocity in the comoving frame to be small compared with the sound speed throughout much of the jet evolution, as long as the Lorentz factor, Γ, is of order a few or larger along the jet axis (Kumar & Granot 2003). This model is expected to be a good approximation for calculating the jet dynamics and the resulting afterglow light curves for the first few days after a GRB.

The second model considers the maximum possible redistribution of energy in the transverse direction so as to reduce the lateral gradient of ϵ. The energy per unit solid angle, $\epsilon(\theta, t)$, is taken to be proportional to the average over the initial distribution of ϵ, $\epsilon(\theta, t_0)$, within the area out to which a sound wave could have traveled from θ since the initial time, t_0. This model is likely to be more accurate in describing the late-time behavior of the jet and the light curves, when the transverse velocity becomes of the same order as the sound speed.

We have calculated light curves for a number of different initial jet structures, which are taken to be power-law profiles at angles larger than some core angle, i.e., $\epsilon \propto \theta^{-a}$ and $\Gamma \propto \theta^{-b}$ for $\theta > \theta_c$. We have considered three different jet profiles, namely, $(a, b) = (2, 0)$, $(2, 2)$, and $(0, 2)$ for a homogeneous external medium, as well as an ambient density falling off as the square of the distance from the center of explosion (i.e., $k = 0$ or 2, where $\rho_{ext} \propto r^{-k}$). We have

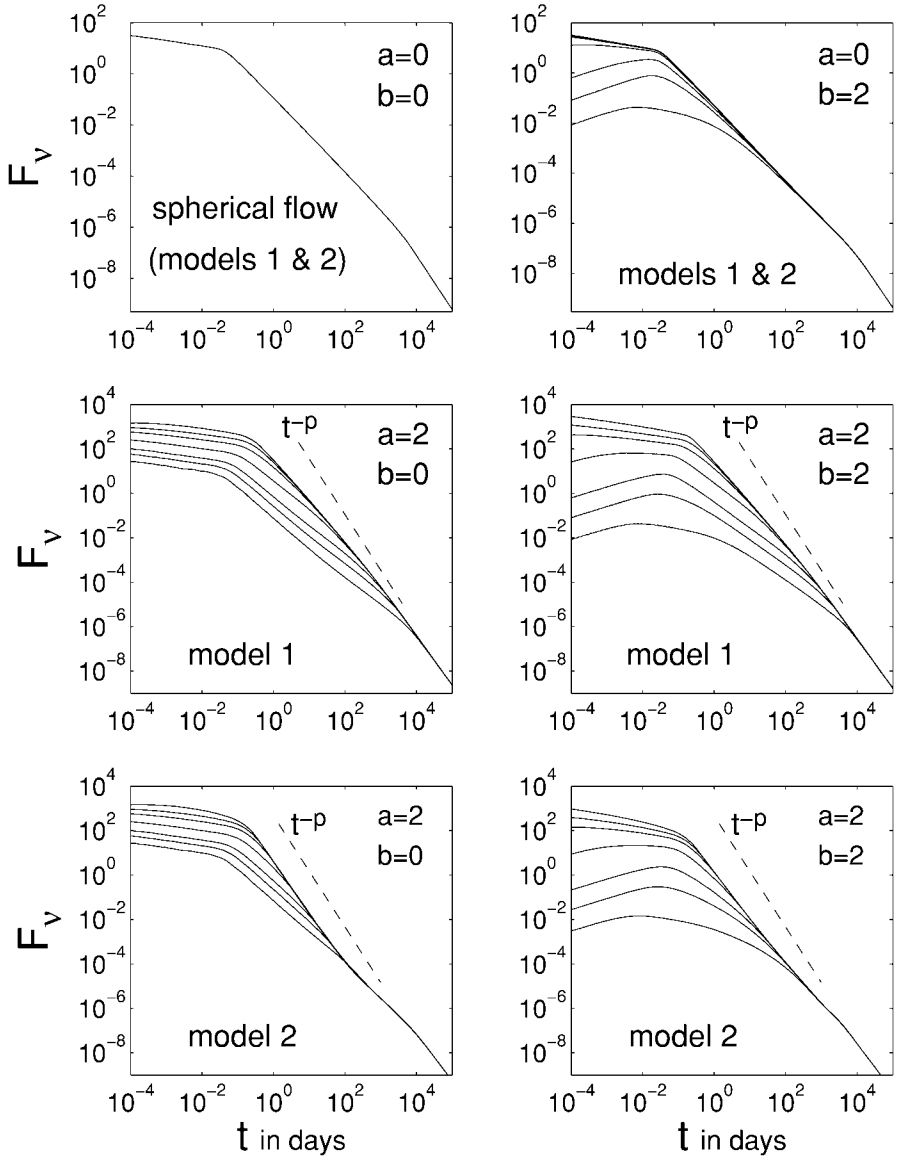

FIG. 8.—Same as Fig. 4, but for an external density $\propto r^{-2}$, corresponding to a stellar wind, with $A = 5 \times 10^{11}$ g cm^{-1}. [*See the electronic edition of the Journal for a color version of this figure.*]

also investigated the dependence of the light curve on the parameter a by calculating the light curves for a uniform density medium by using a constant value of $b = 0$ and three different values of a: $a = 1$, 2, and 3.

The quantitative differences in the light curves calculated using our two models are typically of order unity for all the jet structures we have considered (see Fig. 7). This gives us some confidence that light curves can be calculated with a reasonable accuracy even with a crude modeling of jet dynamics. There are, however, interesting qualitative differences in the light-curve properties depending on how we model jet dynamics. For instance, for $(a, b) = (2, 2)$ and a homogeneous medium ($k = 0$), the temporal index of the light curve, α (defined by $F_\nu \propto t^\alpha$), before the jet break is larger for large viewing angles, $\theta_{\rm obs}$. This effect is much more prominent for model 1, compared with model 2. For $(a, b) = (2, 0)$ and $k = 0$, with model 1 there is a pronounced flattening in the light curve just before the jet break for $\theta_{\rm obs} \gtrsim 3\theta_c$, while for model 2 this effect is much smaller.

There is a significant difference between the two models in the late-time light curves, as we expect: model 1 light curves continue a power-law decline at late times, whereas model 2 light curves show a slight flattening at late times resulting from energy redistribution. See Figures 4, 5, and 7 for a homogeneous external medium with jet structures $(a, b) = (2, 2)$ and (2, 0) and Figures 8 and 9 for the stratified external medium, the particular case of $(a, b) = (2, 0)$. Figures 8 and 9 also show that the break in the light curves for a stratified external medium is very gentle and the change to the power-law index α is small so long as the observer is not too far along the axis: $\theta_{\rm obs}/\theta_c \lesssim 10$. This result is consistent with the work of Kumar & Panaitescu (2000), based on the analysis of a top-hat jet model, so that it is very difficult to see a break in light curves for jets in an r^{-2} medium.

We can learn about the jet structure in GRBs by comparing our theoretical light curves to GRB afterglow observations. For instance, the light curves for $(a, b) = (2, 0)$ and (2, 2) behave very differently prior to the jet break. This can

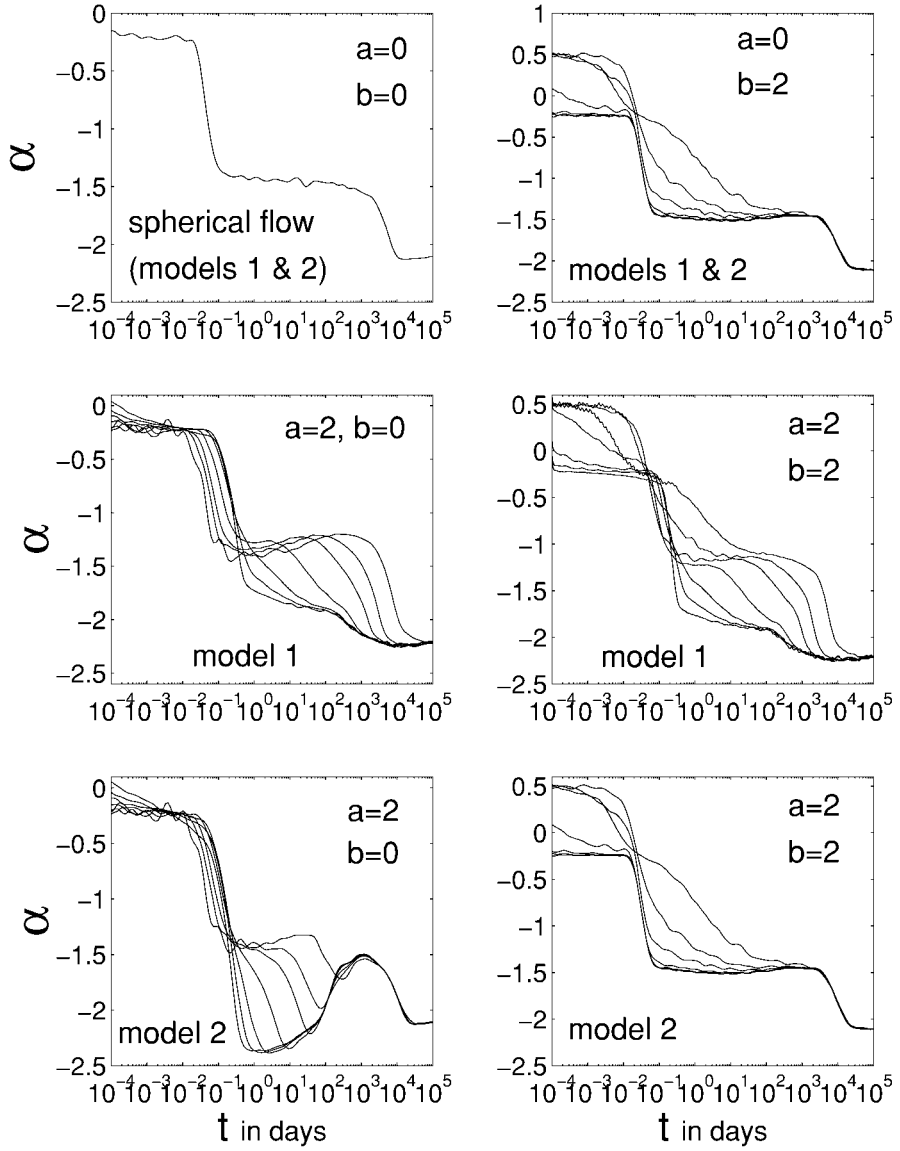

FIG. 9.—Temporal decay slope, α, for the light curves shown in Fig. 8 that are for a stellar wind environment ($k = 2$). [*See the electronic edition of the Journal for a color version of this figure.*]

be used to discriminate between these possibilities (Figs. 4 and 5). For obvious reasons, the light curves for the (0, 2) case are very distinct and similar to a spherically symmetric explosion and do not show a jet break. This jet structure can therefore be ruled out for all GRBs that show a jet break in their afterglow light curves. Clear breaks in the light curves can be seen for a stratified external medium density only when the observer is located far away from the jet axis ($\theta_{\rm obs} \gtrsim 10\theta_c$); however, in this case the GRB will be faint and is likely to be missed in flux-limited triggers for detecting GRBs.

The light curves we obtain for structured jets in many cases show a different qualitative behavior compared with afterglow observations. For example, $k = 2$ does not produce a sufficiently sharp jet break, while for $k = 0$ only $a \approx 2$ produces jet breaks that resemble afterglow observations, and even then it is not clear whether all current afterglow observations can be produced with a universal jet profile, that is, if all GRB jets have the same structure and differ only by our viewing angle, $\theta_{\rm obs}$, with respect to the jet symmetry axis. Our results do indicate, however, that such a universal jet profile would need to have $a \approx 2$ and $0 \lesssim b \lesssim 1$. Whether such a universal jet profile can account for all current afterglow observations will have to be tested by performing detailed fits to afterglow data and will be the subject of a future work. Even if GRB jets do not have a universal structure, a comparison between the observed light curve and theoretical calculations can constrain the jet structure of each GRB separately.

Future afterglow observations should enable us to determine the structure of relativistic jets in GRBs, as well as the properties of the surrounding medium. This will enable us to determine whether the energy release in GRBs is nearly constant or not and whether the observed afterglow light curves and the jet break time are determined by the observer angle with respect to a structured jet or by the opening angle of a top-hat jet.

This work was supported by the Institute for Advanced Study, funds for natural sciences (J. G.).

REFERENCES

Covino, S., et al. 1999, A&A, 348, L1
Frail, D., et al. 2001, ApJ, 562, L55
Ghisellini, G., & Lazzati, D. 1999, MNRAS, 309, L7
Granot, J., Panaitescu, A., Kumar, P., & Woosley, S. E. 2002, ApJ, 570, L61
Granot, J., Piran, T., & Sari, R. 1999, ApJ, 527, 236
Granot, J., et al. 2001, in GRBs in the Afterglow Era, ed. E. Costa, F. Frontera, & J. Hjorth (Berlin: Springer), 312
Guetta, D., & Granot, J. 2003, MNRAS, 340, 115
Königl, A., & Granot, J. 2002, ApJ, 574, 134
Kumar, P., & Granot, J. 2003, ApJ, 591, 1075
Kumar, P., & Panaitescu, A. 2000, ApJ, 541, L9
Lipunov, V. M., Postnov, K. A., & Prokhorov, M. E. 2001, Astron. Rep., 45, 236
Mészáros, P., Rees, M. J., & Wijers, R. A. M. J. 1998, ApJ, 499, 301
Moderski, R., Sikora, M., & Bulik, T. 2000, ApJ, 529, 151
Panaitescu, A., & Kumar, P. 2002, ApJ, 571, 779
Panaitescu, A., & Mészáros, P. 1999, ApJ, 526, 707
Piran, T., Panaitescu, A., Kumar, P., & Piro, L. 2001, ApJ, 560, L167
Rhoads, J. 1997, ApJ, 487, L1
———. 1999, ApJ, 525, 737
Rol, E., et al. 2000, ApJ, 544, 707
Rossi, E., Lazzati, D., & Rees, M. J. 2002, MNRAS, 332, 945
Sari, R. 1999, ApJ, 524, L43
Sari, R., Piran, T., & Halpern, J. P. 1999, ApJ, 519, L17
Sari, R., Piran, T., & Narayan, R. 1998, ApJ, 497, L17
Wijers, R. A. M. J., et al. 1999, ApJ, 523, L33
Zhang, B., & Mészáros, P. 2002, ApJ, 571, 876